ACS Energy LETTERS

Cite This: ACS Energy Lett. 2019, 4, 390−396

http://pubs.acs.org/journal/aelccp

LETTER

Partially Dissociated Water Dimers at the Water−Hematite Interface

Zdenek Jakub,[†] Florian Kraushofer,[†] Magdalena Bichler,[‡] Jan Balajka,[†] Jan Hulva,[†] Jiri Pavelec,[†] Igor Sokolović,[†] Matthias Müllner,[†] Martin Setvin,[†] Michael Schmid,[†] Ulrike Diebold,[†] Peter Blaha,[‡] and Gareth S. Parkinson*[,†]

[†]Institute of Applied Physics, TU Wien, 1040 Vienna, Austria

[‡]Institute of Materials Chemistry, TU Wien, 1060 Vienna, Austria

Supporting Information

ABSTRACT: The oxygen evolution reaction (OER) is thought to occur via a four-step mechanism with *O, *OH, and *OOH as adsorbed intermediates. Linear scaling of the *OH and **OOH adsorption energies is proposed to limit the oxides' efficiency as OER catalysts, but the use of simple descriptors to screen candidate materials neglects potentially important water−water interactions. Here, we use a combination of temperature-programmed desorption (TPD), X-ray photoemission spectroscopy (XPS), noncontact atomic force microscopy (nc-AFM), and density functional theory (DFT)-based computations to show that highly stable HO−H_2O dimer species form at the $(1\bar{1}02)$ facet of hematite; a promising anode material for photoelectrochemical water splitting. The UHV-based results are complemented by measurements following exposure to liquid water and are consistent with prior X-ray scattering results. The presence of strongly bound water agglomerates is generally not taken into account in OER reaction schemes but may play a role in determining the required OER overpotential on metal oxides.

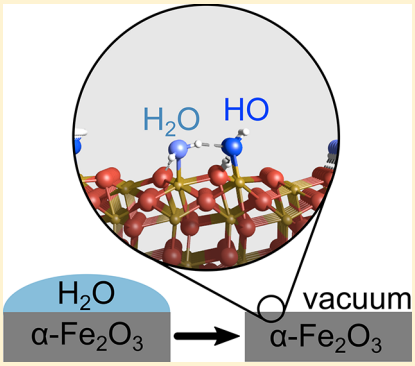

Electrochemical water splitting is an exciting solution for our energy conversion needs, but the overpotential required to initiate the oxygen evolution reaction (OER) prevents this technology from becoming economically viable. The reaction is thought to proceed via a four-step pathway with *O, *OH, and *OOH as adsorbed intermediates (* indicates an adsorbed species).[1] Metal oxides and hydroxides are promising catalysts,[2] but the discovery of a linear scaling between the binding energies of *OH and *OOH is proposed to put a lower limit on the achievable efficiency.[1−5] Computational screening of candidate materials based on descriptors such as the *OH binding energy[3,6] or the orbital occupancy of the metal cation[2,7] has yielded significant success in predicting the materials' OER activity, but to be tractable, these approaches assume a common reaction mechanism on all surfaces and that water−water interactions can be neglected.[8]

Of the proposed schemes, photoelectrochemical (PEC) water splitting has attracted attention because it enables direct conversion of solar energy into chemical energy. Hematite (α-Fe_2O_3) is a highly investigated photoanode material because it has a 2 eV band gap (well-matched to the solar spectrum), is chemically stable, is inexpensive, and is environmentally benign.[9−11] Sluggish OER kinetics are a major bottleneck, however. As long as the exact reaction mechanism remains unknown, it is difficult to understand the cause or tailor a solution. A key step toward understanding this important system, and the OER in general, is to understand the atomic-scale structure of the hematite−water interface.

In this Letter, we study how water adsorbs on one of the most important surfaces of hematite,[12] the $(1\bar{1}02)$ surface. This surface has a comparable surface energy to the more extensively studied (0001) facet[13,14] and is also prevalent on nanomaterials. The $(1\bar{1}02)$ surface is preferable as a model system for our purposes because a monophase (1 × 1) termination can be prepared under ultrahigh vacuum (UHV) conditions,[15,16] and its properties are well-characterized from both an experimental and theoretical point of view. (The atomic structure of (0001), in contrast, is much debated.[17,18]) Interestingly, both surfaces are reported to adsorb a mixture of molecular and dissociated water under UHV conditions,[13,19,20] but the origin of dissociation is unknown.

Here, we use a combination of noncontact atomic force microscopy (nc-AFM), temperature-programmed desorption (TPD), X-ray photoelectron spectroscopy (XPS), and density functional theory (DFT) based computations to show that highly stable, partially dissociated water dimers (HO−H_2O) dominate on the α-$Fe_2O_3(1\bar{1}02)$ surface at all coverages. The

Received: November 29, 2018
Accepted: January 2, 2019
Published: January 2, 2019

DOI: 10.1021/acsenergylett.8b02324
ACS Energy Lett. 2019, 4, 390−396

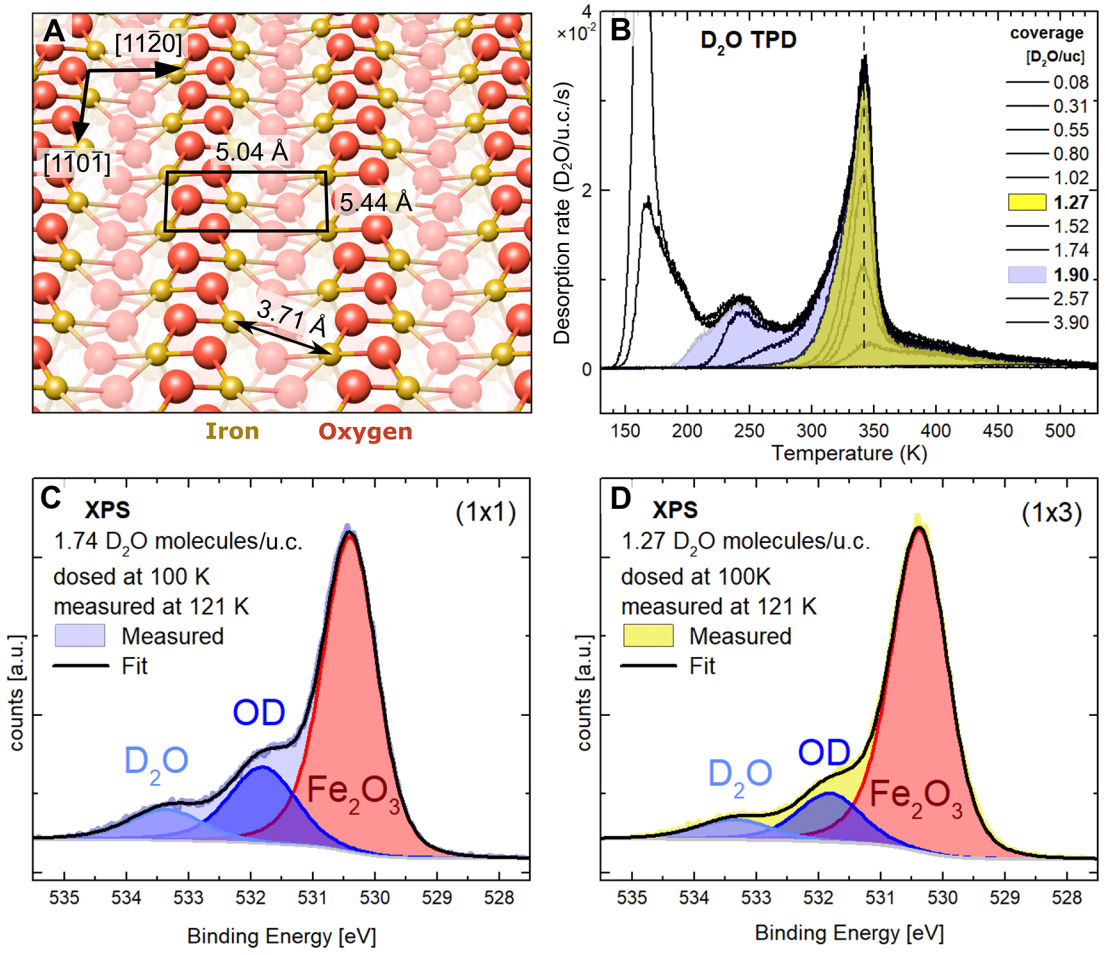

Figure 1. Spectroscopic characterization of water at the α-$Fe_2O_3(1\bar{1}02)$-(1 × 1) surface. (A) Perspective view of the clean α-$Fe_2O_3(1\bar{1}02)$-(1 × 1) surface.[15] The unit cell (uc), marked in black, contains two five-fold-coordinated Fe^{3+} cations (brown) and two three-fold coordinated O^{2-} anions (red). (B) Temperature-programmed desorption (TPD) spectra for D_2O on α-$Fe_2O_3(1\bar{1}02)$-(1 × 1) for various coverages up to 3.9 D_2O/uc. (C,D) X-ray photoemission spectra (monochromatized Al Kα) from the O 1s region for 1.74 and 1.27 D_2O/uc. Both spectra were acquired in grazing emission. The D_2O was dosed at 100 K, and the measurement was performed at 121 K. In both cases, the spectrum shows a peak from lattice O^{2-} anions (530.4 eV) and contributions from molecular D_2O (533.4 eV) and OD (531.8 eV). Fitting the spectra reveals that half of the adsorbed water is dissociated in both cases (see the main text).

dimers form because undercoordinated surface cation sites are sufficiently close for adsorbed water species to develop a strong intermolecular H-bond yet are sufficiently far apart to preclude longer chains. Exposing the surface to liquid water leads to similar results, suggesting that the UHV-prepared surface structure survives immersion. The UHV-derived water dimer model is consistent with the structure of the stable liquid water/α-$Fe_2O_3(1\bar{1}02)$ interface determined in in situ experiments,[21,22] suggesting that partial dissociation may play a previously unforeseen role in water-based surface chemistry of hematite.

The experiments were performed on natural α-$Fe_2O_3(1\bar{1}02)$ single crystals (SurfaceNet GmbH), prepared in UHV to expose a bulk-terminated (1 × 1) surface termination by cycles of 1 keV Ar^+ sputtering and annealing (450 °C, $p_{O_2} = 1 \times 10^{-6}$ mbar). Figure 1A shows a perspective view of the minimum-energy surface structure determined by DFT+U calculations.[15] The (1 × 1) unit cell is bulk-truncated and contains two five-fold-coordinated Fe^{3+} cations and two three-fold-coordinated O^{2-} anions in the surface layer. Figure 1 also shows TPD and XPS data acquired following exposure of the as-prepared surface to a calibrated molecular beam[23] of D_2O at 100 K. The TPD data, acquired using a 1 K/s temperature ramp, resemble those previously shown by Henderson[19] with a major desorption peak at 345 K. This peak saturates at a coverage of 1.27 ± 0.07 D_2O molecules per unit cell (uc), where 1 D_2O/uc corresponds to a coverage of 3.65 × 10^{14} D_2O/cm^2. For higher initial coverages, a shoulder appears at the low-temperature side and develops into a second peak at ~250 K. At lower temperatures, water desorption continues up to a coverage of 1.90 ± 0.10 D_2O/uc, after which a peak corresponding to multilayer ice appears. Saturation of the first monolayer at a coverage of ~2 D_2O/uc can be expected because the (1 × 1) unit cell contains two undercoordinated Fe^{3+} cations to which water molecules can bind (Figure 1A). An inversion analysis[24,25] of the 345 K peak, assuming first-order desorption kinetics, yields a best fit for an adsorption energy of ~1.10 eV, with a pre-exponential factor of 2 × $10^{(15\pm1)}$ s^{-1} (details in the SI). A similar analysis of the higher-coverage ~250 K peak was unsuccessful due do the irregular peak shape.

XPS data (Figure 1C,D) were acquired for D_2O exposures of 1.27 and 1.74 D_2O/uc, which correspond to saturation of the 345 K peak and close to saturation of the 250 K TPD peak.

DOI: 10.1021/acsenergylett.8b02324
ACS Energy Lett. 2019, 4, 390−396

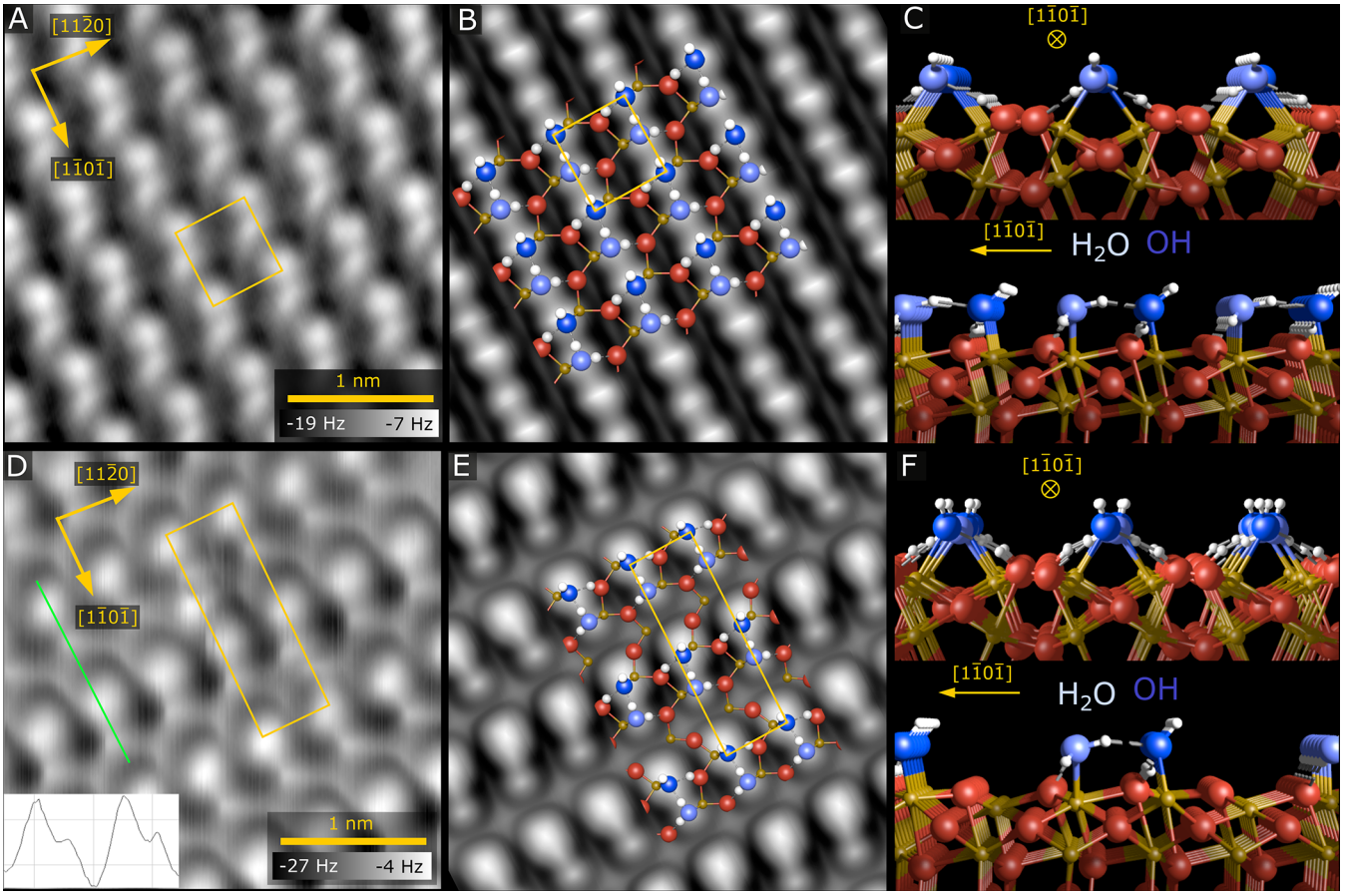

Figure 2. Noncontact atomic force microscopy and PBE+*U* results for H_2O on $Fe_2O_3(1\bar{1}02)$-(1 × 1). (A) Experimental nc-AFM image of the (1 × 1) phase of adsorbed H_2O acquired at 78 K using a CO tip. (B) Simulated nc-AFM image showing the force experienced by a flexible CO tip 7.13 Å above the (1 × 1) phase of adsorbed partially dissociated water dimers. The simulation is based on the minimum-energy PBE +*U* structure, which is shown as an overlay, and in DFT-derived models viewed along the $(1\bar{1}0\bar{1})$ and $(11\bar{2}0)$ directions in panel (C). (D) Experimental nc-AFM image of the (1 × 3) phase of adsorbed H_2O acquired at 4 K using a CO tip. The green line profile shows the four maxima corresponding to two dimer species. (E) Simulated nc-AFM image showing the force experienced by a flexible CO tip 6.68 Å above the (1 × 3) phase of adsorbed partially dissociated water dimers. (F) Models of the minimum-energy DFT structure of the low-coverage phase. In both structures, OH and water are bound to undercoordinated Fe cations (brown), with one $O_{lattice}H$ formed at a surface oxygen (red). The O atoms of the intact and dissociated water molecules are shown in light and dark blue, respectively.

The measurements were performed with grazing emission at 75°, at a sample temperature of 121 K. In addition to the peak at 530.4 eV due to lattice O^{2-} anions, there are two clear contributions at higher binding energy. Fitting the spectra using a Shirley background and three pseudo-Voigt peaks, we identify peaks at 531.8 and 533.4 eV, which are typical for OD and D_2O on metal oxide surfaces.[26,27] Integrating the peak areas, we find that the D_2O/OD ratio is 0.40 for both water coverages. Noting that dissociation results in two hydroxy groups (one so-called terminal $O_{water}D$ adsorbed at a cation site and an $O_{lattice}D$ group at an undercoordinated surface oxygen), this ratio suggests that approximately 45% of the water is molecularly adsorbed. Dissociation by the X-ray beam is ruled out because the same OD/D_2O ratio was obtained in the first and last O 1s scan.

Noncontact AFM experiments were performed in a different vacuum system using an Omicron LTSTM equipped with a Qplus sensor and an in-vacuum preamplifier.[28] Imaging was performed in constant height mode at 78 K and 4 K with a CO-functionalized tip, which produces stable and reproducible conditions for measuring water adsorbed on surfaces.[27,29,30] Figure 2A shows the α-$Fe_2O_3(1\bar{1}02)$-(1 × 1) surface following exposure to 6 L (Langmuir, 1.33×10^{-6} mbar s) of H_2O at 240 K. Judging from the TPD data, these conditions correspond to a maximum coverage of 1.52 H_2O/uc, although we note that there is likely a discrepancy in the temperature measurement in different setups. The resulting image exhibits zigzag rows of protrusions of similar frequency shift running in the $(1\bar{1}0\bar{1})$ direction and has a (1 × 1) periodicity, consistent with one water molecule per surface cation. From the images alone, it is difficult to tell whether the protrusions show H_2O, OH, or both; therefore, we performed theoretical calculations with WIEN2k[31] using the PBE+*U* approach (U_{eff} = 4.0 eV).

The lowest-energy (1 × 1) configuration (Figure 2C) (E_{ad} = 1.02 eV/H_2O) based on partially dissociated water dimers is clearly favored over intact (0.84 eV/H_2O) or fully dissociated (0.92 eV/H_2O) water monomers. A water molecule and a terminal OH adsorb atop surface Fe cations (brown), completing their octahedral coordination environment. A hydrogen bond of 1.56 Å forms between the water and the terminal OH species on neighboring cations along the row. The H liberated by the dissociation forms an $O_{lattice}H$ with an undercoordinated surface O atom and forms a hydrogen bond (1.68 Å) back to the O of the dissociated water molecule. In

DOI: 10.1021/acsenergylett.8b02324
ACS Energy Lett. 2019, 4, 390−396

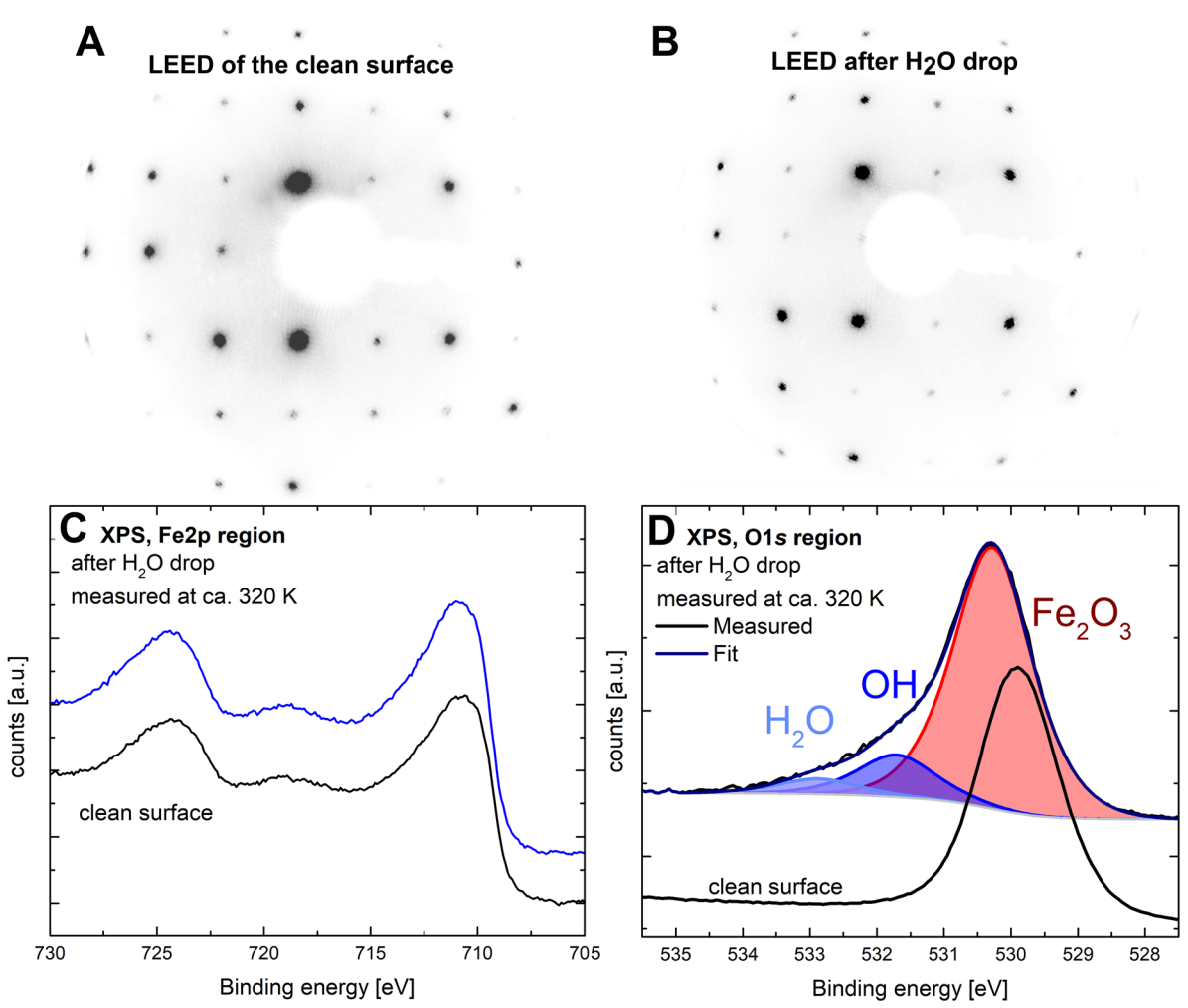

Figure 3. LEED patterns of the clean surface (A) and after exposure to a liquid water drop (B), both acquired at 120 eV. (C,D) XPS spectra (Mg Kα) of the Fe 2p and O 1s regions before (black) and after (blue) exposure to liquid water.

Figure 2B, we show a simulation of the AFM contrast using the flexible CO tip model as implemented in the Probe Particle Model.[32] Details of the calculations and the simulation approach are included in the SI.

The TPD results suggest that a phase more favorable than the full-coverage (1 × 1) structure contains ~1.27 D_2O/uc (peak at 345 K). The nc-AFM image shown in Figure 2D was acquired at 4 K after the as-prepared α-$Fe_2O_3(1\bar{1}02)$-(1 × 1) surface was exposed to 10 L of H_2O at 300 K; again a CO-functionalized tip was used in constant-height mode. The image exhibits two types of protrusions, one slightly smaller than the other. These features form pairs along the $(1\bar{1}0\bar{1})$ direction, with the axes of the pairs slightly rotated in alternating directions. This creates a (1 × 3) periodicity with four protrusions per (1 × 3) cell. If each of these protrusions is water or $O_{water}H$, a full (1 × 3) overlayer contains 1.33 D_2O/uc, which nicely corresponds to the 1.27 ± 0.07 D_2O/uc coverage determined from TPD.

DFT+U calculations based on four water molecules per (1 × 3) unit cell find the most stable structure (1.07 eV/H_2O) to be two partially dissociated water dimers. Between two dimers, one Fe cation site is left vacant. As before, the nc-AFM simulation based on this structure (Figure 2E) agrees well with the experimental image (Figure 2D) and allows identifation of the larger bright feature as the terminal OH group and the smaller bright feature as the water molecule.

Our experimental and theoretical data combined show that a partially dissociated water dimer is the most stable form of adsorbed water on the α-$Fe_2O_3(1\bar{1}02)$ surface under UHV conditions. Such species have now been found on several metal oxide surfaces[26,27,33−38] and thus appear to be common. The cooperative origin[39] of their stability was discussed in detail in a recent paper on the water/Fe_3O_4(001) system,[27] but it is important to note that such species will form when undercoordinated surface cations are in close proximity such that an intermolecular H bond can form between strongly adsorbed water molecules. This bond is significantly strengthened when the H-bond receiver dissociates to form a negatively charged OH species, and this in turn causes the H-bond-donating water molecule to interact more strongly with the surface cation. For this to happen, undercoordinated oxygen atoms are required to receive the liberated proton and form a stable $O_{surface}H$ group. Because these conditions are met on many oxide surfaces, partially dissociated water dimers are often reported as highly stable structures, even though at higher coverages often more complex structures prevail. The cooperativity effect holds in the longer-range structures too and affects the coverage-dependent reactivity of surfaces

DOI: 10.1021/acsenergylett.8b02324
ACS Energy Lett. 2019, 4, 390−396

toward water dissociation, as has been recently observed on TiO_2.[38]

While our ultrahigh-vacuum experiments are an ideal complement to theory, they do not tell whether (a) the UHV-prepared surface would be relevant or even stable in liquid water or (b) at least similar species might form in that very different environment. As a first step toward answering this question, we exposed the UHV-prepared α-$Fe_2O_3(1\bar{1}02)$-(1 × 1) surface to a drop of ultrapure liquid water. The experiment was performed in a new water-dosing setup, interfaced by a gate valve to a regular UHV chamber containing equipment for STM, LEED, and XPS.[40] First, ultrapure water is leaked into a small side chamber containing a liquid N_2-cooled cold-finger directly above the sample stage. When a small icicle is formed, the valve to the water is closed, the chamber is re-evacuated, and the clean sample is introduced from the main UHV chamber. The coldfinger is warmed, the icicle melts, and liquid water drops onto the sample surface. The side chamber is then re-evacuated, the water evaporates, and the sample is moved back to the main UHV chamber for analysis.

Figure 3 shows LEED patterns and XPS spectra obtained following UHV preparation and after exposure to liquid H_2O for ca. 30 s at room temperature. Both LEED images show a (1 × 1) periodicity, consistent with the bulk-truncated surface (Figure 1A). Also, ambient AFM measurements following exposure to water for 1 h (see the SI) show no morphological changes such as pits or islands that might be linked to dramatic change of the surface structure. O 1s and Fe 2p XPS spectra acquired at 320 K resemble those obtained at 121 K, with contributions from lattice O^{2-}, OH and H_2O. The intensity of the water-related features decreased over the course of the measurement because the measurement temperature (~320 K) is in the leading edge of the 345 K TPD peak. Interestingly, the H_2O/OH ratio also changed from 0.37 to 0.21, indicating a higher fraction of dissociated water with decreasing coverage. In view of the TPD tail above ~370 K (Figure 1B), we attribute the excess dissociated signal at least partly to steps or defect sites; at low coverage, these outweigh the partially dissociated dimers at regular lattice sites. We also note that a previous TPD study of the water/α-$Fe_2O_3(1\bar{1}02)$ system showed significant oxygen exchange with the surface in the 345 K peak,[19] suggesting a nontrivial desorption mechanism. The barrier for this process, which is presently unknown but seems to obey first-order kinetics, will ultimately define the temperature at which desorption will occur in TPD and most likely underlies a significant portion of the 100 K temperature difference observed there.

The liquid exposure experiment suggests that the UHV-prepared surface survives immersion in liquid water and that partially dissociated water remains when the sample is returned to UHV. It is useful to compare our results to surface X-ray diffraction experiments performed on α-$Fe_2O_3(1\bar{1}02)$ single crystals covered with a layer of liquid water.[21,22] In these experiments, the sample was prepared by wet chemical etching followed by annealing in air, which produces a stoichiometric bulk termination. Structural refinements suggested that oxygen atoms complete the octahedral coordination shell of outermost Fe^{3+} cations, i.e., occupying the same positions as those shown for the oxygen atoms in our model (blue in Figure 2B,C,E,F). This surface was stable in water for (at least) 4 days,[21] and in situ measurements of the immersed sample suggested that further water ordering continues at least 1 nm from the surface. Unfortunately, X-ray diffraction is not sensitive to the location of the H atoms; therefore, it is impossible to say whether these oxygen atoms result from partially dissociated water or not. Interestingly, though, there is evidence from ambient-pressure XPS experiments that OH can exist at the interface following the condensation of multilayer water on the UHV-prepared α-$Fe_2O_3(0001)$ surface,[13] and a recent study of immersed hematite nanoparticles suggests that OH remains adsorbed at the interface in liquid water.[41] As such, it seems reasonable to suggest that partially dissociated dimers may form at the aqueous interface and thus that water−water interactions could be important in the OER. While it is difficult to know the effect that these structures might have on the OER overpotential in this case, it is clear that the stability of the *OH bound in the reported water dimers differs significantly from the stability of an isolated *OH bound to the surface. Screening materials based on this parameter will thus lead to incorrect placements on the OER volcano plot and may lead us to discard promising materials. It is also difficult to know how the presence of strongly bound intermediates would change the reaction mechanism and thus the relevance of the scaling relations. Because strong water−water effects appear to be a common feature on metal oxide surfaces, it makes sense to pursue the answer to these questions for a few select cases. Given its well-characterized surface and interface, we suggest that the α-$Fe_2O_3(1\bar{1}02)$ system would be a well-suited test bed for more sophisticated computational modeling of this important reaction.

■ ASSOCIATED CONTENT

Supporting Information

The Supporting Information is available free of charge on the ACS Publications website at DOI: 10.1021/acsenergylett.8b02324.

Experimental and computational details, analysis of the TPD data, oxygen exchange upon water desorption, additional STM and nc-AFM data, nc-AFM contrast simulations, and additional high-pressure exposure experiments (PDF)

■ AUTHOR INFORMATION

Corresponding Author

*E-mail: parkinson@iap.tuwien.ac.at.

ORCID

Zdenek Jakub: 0000-0001-9538-9087
Florian Kraushofer: 0000-0003-1314-9149
Jan Balajka: 0000-0001-7101-1055
Martin Setvin: 0000-0002-1210-7740
Ulrike Diebold: 0000-0003-0319-5256
Gareth S. Parkinson: 0000-0003-2457-8977

Notes

The authors declare no competing financial interest.

■ ACKNOWLEDGMENTS

The authors gratefully acknowledge funding through the following projects from the Austrian Science Fund FWF: START-Prize Y 847-N20 (F.K., J.H., G.S.P.), Wittgenstein Prize Z 250 (U.D.), the Special Research Project "Vienna Computational Materials Laboratory" ViCoM (F41 (P.B.)), the Doctoral College Solids4Fun (M.B., J.B., I.S.), as well as the Doctoral College TU-D (Z.J.). The computational results

DOI: 10.1021/acsenergylett.8b02324
ACS Energy Lett. 2019, 4, 390−396

presented have been achieved using the Vienna Scientific Cluster (VSC).

REFERENCES

(1) Koper, M. T. M. Thermodynamic Theory of Multi-Electron Transfer Reactions: Implications for Electrocatalysis. *J. Electroanal. Chem.* **2011**, *660*, 254−260.

(2) Hong, W. T.; Risch, M.; Stoerzinger, K. A.; Grimaud, A.; Suntivich, J.; Shao-Horn, Y. Toward the Rational Design of Non-Precious Transition Metal Oxides for Oxygen Electrocatalysis. *Energy Environ. Sci.* **2015**, *8*, 1404−1427.

(3) Man, I. C.; Su, H.-Y.; Calle-Vallejo, F.; Hansen, H. A.; Martínez, J. I.; Inoglu, N. G.; Kitchin, J.; Jaramillo, T. F.; Nørskov, J. K.; Rossmeisl, J. Universality in Oxygen Evolution Electrocatalysis on Oxide Surfaces. *ChemCatChem* **2011**, *3*, 1159−1165.

(4) Christensen, R.; Hansen, H. A.; Dickens, C. F.; Nørskov, J. K.; Vegge, T. Functional Independent Scaling Relation for ORR/OER Catalysts. *J. Phys. Chem. C* **2016**, *120*, 24910−24916.

(5) Rossmeisl, J.; Qu, Z. W.; Zhu, H.; Kroes, G. J.; Nørskov, J. K. Electrolysis of Water on Oxide Surfaces. *J. Electroanal. Chem.* **2007**, *607*, 83−89.

(6) García-Mota, M.; Vojvodic, A.; Metiu, H.; Man, I. C.; Su, H.-Y.; Rossmeisl, J.; Nørskov, J. K. Tailoring the Activity for Oxygen Evolution Electrocatalysis on Rutile TiO_2(110) by Transition-Metal Substitution. *ChemCatChem* **2011**, *3*, 1607−1611.

(7) Suntivich, J.; May, K. J.; Gasteiger, H. A.; Goodenough, J. B.; Shao-Horn, Y. A Perovskite Oxide Optimized for Oxygen Evolution Catalysis from Molecular Orbital Principles. *Science* **2011**, *334*, 1383.

(8) Govindarajan, N.; García-Lastra, J. M.; Meijer, E. J.; Calle-Vallejo, F. Does the Breaking of Adsorption-Energy Scaling Relations Guarantee Enhanced Electrocatalysis? *Curr. Opin. Electrochem.* **2018**, *8*, 110−117.

(9) Sivula, K.; Le Formal, F.; Grätzel, M. Solar Water Splitting: Progress Using Hematite (α-Fe_2O_3) Photoelectrodes. *ChemSusChem* **2011**, *4*, 432−449.

(10) Iandolo, B.; Wickman, B.; Zorić, I.; Hellman, A. The Rise of Hematite: Origin and Strategies to Reduce the High Onset Potential for the Oxygen Evolution Reaction. *J. Mater. Chem. A* **2015**, *3*, 16896−16912.

(11) Tamirat, A. G.; Rick, J.; Dubale, A. A.; Su, W.-N.; Hwang, B.-J. Using Hematite for Photoelectrochemical Water Splitting: A Review of Current Progress and Challenges. *Nanoscale Horiz.* **2016**, *1*, 243−267.

(12) Stirner, T.; Scholz, D.; Sun, J. Ab Initio Simulation of Structure and Surface Energy of Low-Index Surfaces of Stoichiometric α-Fe_2O_3. *Surf. Sci.* **2018**, *671*, 11−16.

(13) Yamamoto, S.; Kendelewicz, T.; Newberg, J. T.; Ketteler, G.; Starr, D. E.; Mysak, E. R.; Andersson, K. J.; Ogasawara, H.; Bluhm, H.; Salmeron, M.; Brown, G. E.; Nilsson, A. Water Adsorption on α-Fe_2O_3(0001) at near Ambient Conditions. *J. Phys. Chem. C* **2010**, *114*, 2256−2266.

(14) von Rudorff, G. F.; Jakobsen, R.; Rosso, K. M.; Blumberger, J. Hematite(001)-Liquid Water Interface from Hybrid Density Functional-Based Molecular Dynamics. *J. Phys.: Condens. Matter* **2016**, *28*, 394001.

(15) Kraushofer, F.; Jakub, Z.; Bichler, M.; Hulva, J.; Drmota, P.; Weinold, M.; Schmid, M.; Setvin, M.; Diebold, U.; Blaha, P.; Parkinson, G. S. Atomic-Scale Structure of the Hematite α-$Fe_2O_3(1\bar{1}02)$ "R-Cut" Surface. *J. Phys. Chem. C* **2018**, *122*, 1657−1669.

(16) Henderson, M. A. Insights into the (1 × 1)-to-(2 × 1) Phase Transition of the α-Fe_2O_3(012) Surface Using EELS, LEED and Water TPD. *Surf. Sci.* **2002**, *515*, 253−262.

(17) Parkinson, G. S. Iron Oxide Surfaces. *Surf. Sci. Rep.* **2016**, *71*, 272−365.

(18) Kuhlenbeck, H.; Shaikhutdinov, S.; Freund, H.-J. Well-Ordered Transition Metal Oxide Layers in Model Catalysis − a Series of Case Studies. *Chem. Rev.* **2013**, *113*, 3986−4034.

(19) Henderson, M. A.; Joyce, S. A.; Rustad, J. R. Interaction of Water with the (1 × 1) and (2 × 1) Surfaces of α-Fe_2O_3(012). *Surf. Sci.* **1998**, *417*, 66−81.

(20) Wang, R. B.; Hellman, A. Initial Water Adsorption on Hematite (α-Fe_2O_3) (0001): A DFT + U Study. *J. Chem. Phys.* **2018**, *148*, No. 094705.

(21) Catalano, J. G.; Fenter, P.; Park, C. Interfacial Water Structure on the (012) Surface of Hematite: Ordering and Reactivity in Comparison with Corundum. *Geochim. Cosmochim. Acta* **2007**, *71*, 5313−5324.

(22) Tanwar, K. S.; Catalano, J. G.; Petitto, S. C.; Ghose, S. K.; Eng, P. J.; Trainor, T. P. Hydrated α-Fe_2O_3 $(1\bar{1}02)$ Surface Structure: Role of Surface Preparation. *Surf. Sci.* **2007**, *601*, L59−L64.

(23) Pavelec, J.; Hulva, J.; Halwidl, D.; Bliem, R.; Gamba, O.; Jakub, Z.; Brunbauer, F.; Schmid, M.; Diebold, U.; Parkinson, G. S. A Multi-Technique Study of CO_2 Adsorption on Fe_3O_4 Magnetite. *J. Chem. Phys.* **2017**, *146*, No. 014701.

(24) Tait, S. L.; Dohnálek, Z.; Campbell, C. T.; Kay, B. D. N-Alkanes on MgO(100). I. Coverage-Dependent Desorption Kinetics of N-Butane. *J. Chem. Phys.* **2005**, *122*, 164707.

(25) Hulva, J.; Jakub, Z.; Novotny, Z.; Johansson, N.; Knudsen, J.; Schnadt, J.; Schmid, M.; Diebold, U.; Parkinson, G. S. Adsorption of CO on the Fe_3O_4(001) Surface. *J. Phys. Chem. B* **2018**, *122*, 721−729.

(26) Mu, R.; Zhao, Z.-j.; Dohnálek, Z.; Gong, J. Structural Motifs of Water on Metal Oxide Surfaces. *Chem. Soc. Rev.* **2017**, *46*, 1785−1806.

(27) Meier, M.; Hulva, J.; Jakub, Z.; Pavelec, J.; Setvin, M.; Bliem, R.; Schmid, M.; Diebold, U.; Franchini, C.; Parkinson, G. S. Water Agglomerates on Fe_3O_4(001). *Proc. Natl. Acad. Sci. U. S. A.* **2018**, *115*, E5642−E5650.

(28) Huber, F.; Giessibl, F. J. Low Noise Current Preamplifier for Qplus Sensor Deflection Signal Detection in Atomic Force Microscopy at Room and Low Temperatures. *Rev. Sci. Instrum.* **2017**, *88*, No. 073702.

(29) Shiotari, A.; Sugimoto, Y. Ultrahigh-Resolution Imaging of Water Networks by Atomic Force Microscopy. *Nat. Commun.* **2017**, *8*, 14313.

(30) Peng, J.; Guo, J.; Hapala, P.; Cao, D.; Ma, R.; Cheng, B.; Xu, L.; Ondráček, M.; Jelínek, P.; Wang, E.; Jiang, Y. Weakly Perturbative Imaging of Interfacial Water with Submolecular Resolution by Atomic Force Microscopy. *Nat. Commun.* **2018**, *9*, 122.

(31) K. S. Blaha, P.; Schwarz, K.; Madsen, G.; Kvasnicka, D.; Luitz, J. *Wien2k: An Augmented Plane Wave Plus Local Orbitals Program for Calculating Crystal Properties*; Vienna University of Technology, 2001.

(32) Hapala, P.; Kichin, G.; Wagner, C.; Tautz, F. S.; Temirov, R.; Jelínek, P. Mechanism of High-Resolution STM/AFM Imaging with Functionalized Tips. *Phys. Rev. B: Condens. Matter Mater. Phys.* **2014**, *90*, No. 085421.

(33) Mirabella, F.; Zaki, E.; Ivars-Barceló, F.; Li, X.; Paier, J.; Sauer, J.; Shaikhutdinov, S.; Freund, H.-J. Cooperative Formation of Long-Range Ordering in Water Ad-Layers on Fe_3O_4 (111) Surfaces. *Angew. Chem., Int. Ed.* **2018**, *57*, 1409−1413.

(34) Mu, R.; Cantu, D. C.; Glezakou, V.-A.; Lyubinetsky, I.; Rousseau, R.; Dohnálek, Z. Deprotonated Water Dimers: The Building Blocks of Segmented Water Chains on Rutile RuO_2(110). *J. Phys. Chem. C* **2015**, *119*, 23552−23558.

(35) Mu, R.; Cantu, D. C.; Lin, X.; Glezakou, V.-A.; Wang, Z.; Lyubinetsky, I.; Rousseau, R.; Dohnálek, Z. Dimerization Induced Deprotonation of Water on RuO_2(110). *J. Phys. Chem. Lett.* **2014**, *5*, 3445−3450.

(36) Kan, H. H.; Colmyer, R. J.; Asthagiri, A.; Weaver, J. F. Adsorption of Water on a PdO(101) Thin Film: Evidence of an Adsorbed HO−H_2O Complex. *J. Phys. Chem. C* **2009**, *113*, 1495−1506.

(37) Dementyev, P.; Dostert, K.-H.; Ivars-Barceló, F.; O'Brien, C. P.; Mirabella, F.; Schauermann, S.; Li, X.; Paier, J.; Sauer, J.; Freund, H.-J. Water Interaction with Iron Oxides. *Angew. Chem., Int. Ed.* **2015**, *54*, 13942−13946.

DOI: 10.1021/acsenergylett.8b02324
ACS Energy Lett. 2019, 4, 390−396

(38) Yang, W.; Wei, D.; Jin, X.; Xu, C.; Geng, Z.; Guo, Q.; Ma, Z.; Dai, D.; Fan, H.; Yang, X. Effect of the Hydrogen Bond in Photoinduced Water Dissociation: A Double-Edged Sword. *J. Phys. Chem. Lett.* **2016**, *7*, 603−608.
(39) Schiros, T.; Ogasawara, H.; Näslund, L. Å.; Andersson, K. J.; Ren, J.; Meng, S.; Karlberg, G. S.; Odelius, M.; Nilsson, A.; Pettersson, L. G. M. Cooperativity in Surface Bonding and Hydrogen Bonding of Water and Hydroxyl at Metal Surfaces. *J. Phys. Chem. C* **2010**, *114*, 10240−10248.
(40) Balajka, J.; Pavelec, J.; Komora, M.; Schmid, M.; Diebold, U. Apparatus for Dosing Liquid Water in Ultrahigh Vacuum. *Rev. Sci. Instrum.* **2018**, *89*, No. 083906.
(41) Ali, H.; Seidel, R.; Pohl, M. N.; Winter, B. Molecular Species Forming at the α-Fe_2O_3 Nanoparticle−Aqueous Solution Interface. *Chem. Sci.* **2018**, *9*, 4511−4523.

DOI: 10.1021/acsenergylett.8b02324
ACS Energy Lett. 2019, 4, 390−396